Crista Volume Measured from 3D Reconstruction of Weightbearing CT Scans Shows a Relationship to Sesamoid Station

by

Audrey Jean Clarke

B.S. Mechanical Engineering, University of Pittsburgh, 2019

Submitted to the Graduate Faculty of the

Swanson School of Engineering in partial fulfillment

of the requirements for the degree of

Master of Science in Mechanical Engineering

University of Pittsburgh

2021

UNIVERSITY OF PITTSBURGH

SWANSON SCHOOL OF ENGINEERING

This thesis was presented

by

Audrey Jean Clarke

It was defended on

April 1, 2021

and approved by

Anne Robertson PhD, Professor, Mechanical Engineering and Materials Science, Bioengineering
Department

William Clark PhD, Professor, Mechanical Engineering and Materials Science

Thesis Advisor: Mark C. Miller PhD, Associate Research Professor, Mechanical Engineering
and Materials Science

Crista Volume Measured from 3D Reconstruction of Weightbearing CT Scans Shows a Relationship to Sesamoid Station

Audrey Jean Clarke, MS

University of Pittsburgh, 2021

The hallux valgus (HV) deformity results in progressive subluxation of the sesamoids from their position (station) under the plantar surface of the first metatarsal head. This subluxation may result in erosion of the crista that separates the sesamoid grooves due to contact with the tibial sesamoid during weightbearing. While previous work using weightbearing CT (WBCT) scans has suggested that tibial sesamoid position is associated with degenerative change of the sesamoid metatarsal joint (Katsui *FAI*), no studies have quantified the relationship between sesamoid metatarsal degenerative changes and sesamoid subluxation. The purpose of the current investigation is to examine the relationship of the volume of the crista to first metatarsal pronation and sesamoid station, using three-dimensional models of patients' deformities created from WBCT scans.

Thirty-nine HV patients and nine normal subjects underwent weightbearing or simulated weightbearing CT (WBCT) imaging. Crista volume was determined using a line drawn to connect the nadir of each sulcus on either side of the intersesamoidal crista for the length of the crista. WBCT scans were used to establish sesamoid position using a four-stage scale (Kim *FAI* 2015) and quantify first metatarsal pronation using 3D reconstructions as previously described (Campbell *FAI* 2018).

Our study found that HV patients have significantly lower mean crista volumes compared to normal patients. Crista volume was strongly correlated with sesamoid subluxation/station,

which suggests that tibial sesamoid subluxation results in erosion of the crista. In contrast, the pronation deformity was not associated with crista volume demonstrating that the degenerative changes of the sesamoid metatarsal are not related to the rotational deformity of the first metatarsal. This supports the hypothesis that tibial sesamoid subluxation may result in osteoarthritis of the sesamoid metatarsal joint and may be an overlooked source of pain in HV. These results are the first to demonstrate that medial sesamoid subluxation as determined by sesamoid station results in erosion of the crista.

Table of Contents

List of Tables

List of Figures

Preface

       I would like to thank my thesis advisor Dr. Mark Miller for advising me through the process of obtaining a graduate degree. I would like to acknowledge my supportive family, friends, and professors for helping me get to this point in my life. A very special thanks to my mom, dad, Ethan Linderman, and Zachary Yoder.

1.0 Introduction

1.1 What is hallux valgus?

Hallux Valgus (HV), more commonly known as a bunion, is one of the most common foot deformities that causes forefoot pain [1]. HV is a progressive deformity that begins with the great toe deviating laterally and the first metatarsal deviating medially. HV is associated with foot pain, impaired balance, increased risk of falling, impaired gait patterns, and overall a decreased quality of life [2, 3]. The severity of HV is most commonly evaluated radiographically by two planar angles. These angles are called the intermetatarsal angle (IMA), the angle between the first and second metatarsal, and the hallux valgus angle (HVA), the angle between the first metatarsal and first phalanx (Figure 1).

Treatment options for HV include non-surgical and surgical options. The most popular non-surgical treatment options include insoles, shoes with a wide toe-box, physical therapy, and anti-inflammatory drugs. Non-surgical treatment will not correct the deformity but can provide temporary relief to symptoms. However, surgical treatment can be used, and there are over 100 different surgical techniques that have been used to correct the deformity. The appearance and severity of the deformity determines which surgical treatment is to be used [4]. If the proper surgical treatment is chosen incorrectly, recurrence of the deformity is possible[5].
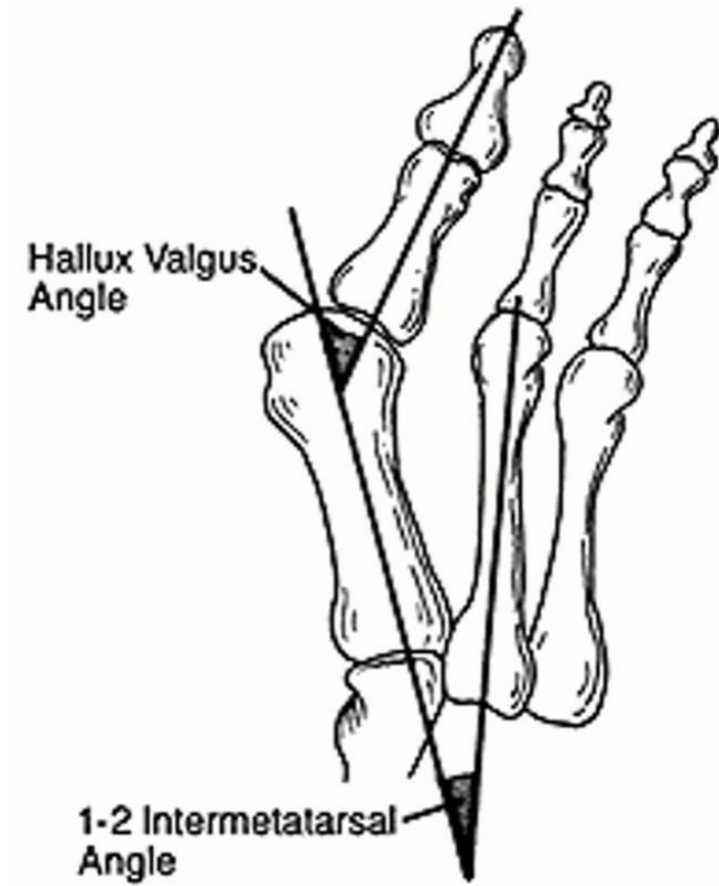
Figure 1: Radiographic meaasurements of hallux valgus [6].

1.2 Prevalence

Hallux valgus is estimated to affect 23% of adults aged 18-65 years, and that number increases to 35.7% in the elderly population aged 65 years and up. Prevalence of HV increases with age and gender. Research shows that HV affects 30% of the female population, while only affecting 13% of the male population[1].

1.3 Anatomic Planes and Direction

The body is broken into sections in terms of three anatomical planes – sagittal, coronal, and transverse. The sagittal plane runs from the front to back of the body, the coronal plane runs through the side of the body, and the transverse plane runs through the mid-section (Figure 2).
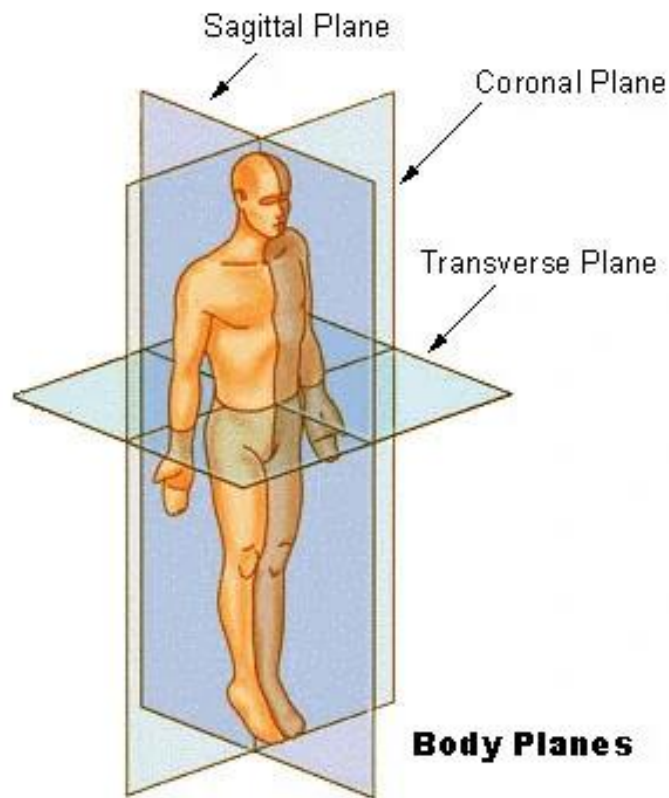
Figure 2: Anatomic planes[7].

The front of the body is referred to as anterior, and the back of the body is referred to as posterior. Parts of the body further from the body are described as distal, and parts closer to the body are proximal. Medial is close to the midline of the body, and lateral is away from the body or towards the edge (Figure 3).

3
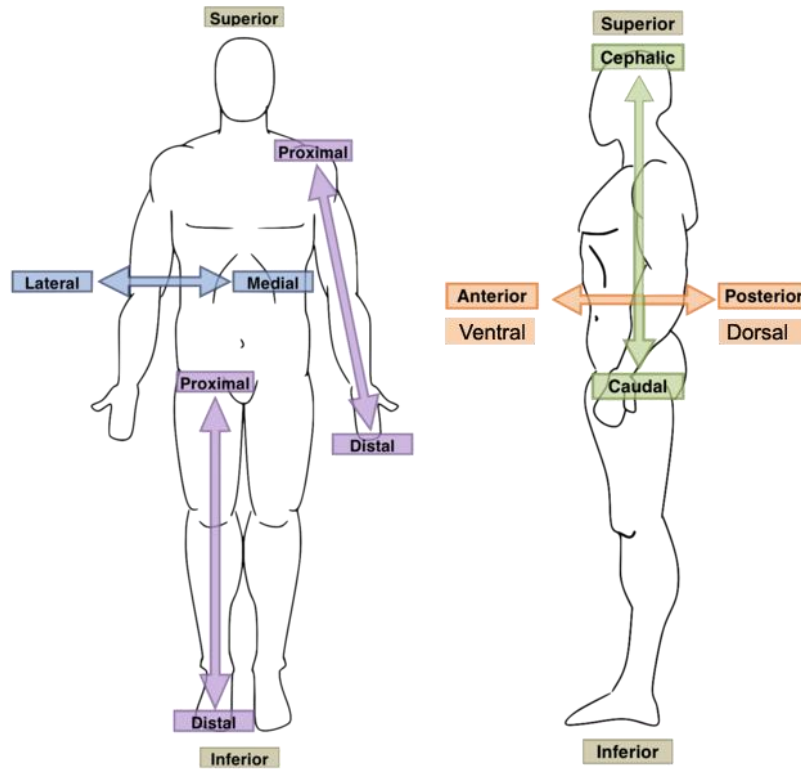
Figure 3: Anatomic direction[8].

1.4 Motivation and Goals

The high prevalence of HV results in a need to understand the mechanical function of the structure better. While the kinematics of HV are understood, the root cause is still unclear. It is hypothesized that the pain experienced from a bunion is caused when the intersesamoid ridge, separating the two sesamoids, is broken down by pressure during abnormal contact with the sesamoids. The purpose of the current investigation is to examine the erosion of the intersesamoid ridge separating the sesamoids and show that it is directly related to sesamoid subluxation, intermetatarsal angle, hallux valgus angle and first metatarsal pronation in HV deformities. A study

that considers crista volume and sesamoid station will provide a better idea of the progression of

HV and improved pre-operative planning.

2.0 Clinical Background on Hallux Valgus

2.1 Associated Factors

Research has shown that hallux valgus can be congenital or acquired. Congenital hallux valgus is inherited. Inheritable factors that can play a role in HV are hypermobility, arch height, and arthritis[9]. Acquired hallux valgus develops over time and can be attributed to tight fitting shoes[10]. Tight shoes can force the foot into unnatural positions and change the gait pattern of the user[11]. Hallux valgus is much more prevalent in females because of the fashionable and tight fitting shoes they tend to wear (e.g. High heels)[12].

2.2 Anatomy of the Foot

In hallux valgus the first proximal phalanx deviates laterally and the distal end of the first metatarsal drifts medially. This deformity affects the alignment of the first metatarsophalangeal (MTP) joint. MA medial and lateral sesamoid bone, contained within the tendons of flexor hallucis brevis (FHB), lie beneath the head of the first metatarsal. An intersesamoid ridge, known as the crista, separates the medial and lateral sesamoids. In a normal foot each sesamoid articulates with a separate groove beneath the surface of the first metatarsal head[13]. The adductor hallucis (AdH) tendon and abductor hallucis (AbH) tendon both play a role in anchoring the sesamoids so that they do not drift medially with the metatarsal head (Figure 4). When the MTP joint becomes compromised, the base of the proximal phalanx pushes the metatarsal head medialward. As the

metatarsal head is displaced, it slides out of the sesamoid apparatus and the metatarsal head sits on top of the medial sesamoid and the lateral sesamoid begins to drift medially. The crista under the metatarsal head is then gradually eroded by the sesamoids[14].

The balance of the forefoot becomes compromised once the sesamoids drift medially[15]. HV does not occur in a series of sequential steps, but rather steps in parallel. As the first metatarsal head deviates medially, the AbH tendon is pulled under the metatarsal head. The proximal phalanx remains attached to the AdH and the lateral sesamoid. As the metatarsal head is pulled medially and the base of the proximal phalanx is held in place, the bone is forced to rotate along its longitudinal axis at the pivot point of the AdH tendon. These forces cause pronation of the great toe[14].
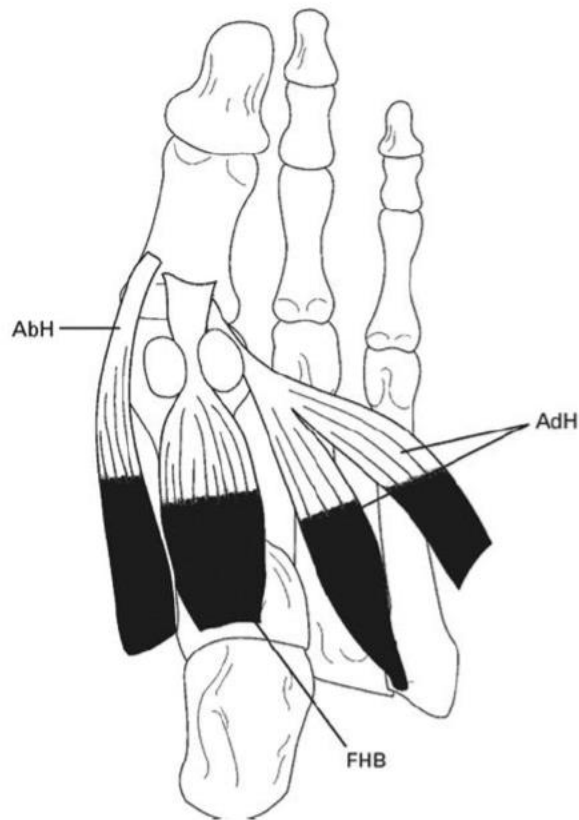
Figure 4: Anatomy of the MTP joint [16].

2.3 Radiographic Assessment

Hallux valgus is usually assessed by measurements taken on plain film images. A plain film image is a two-dimensional radiograph, otherwise known as an X-ray. Anteroposterior (AP), lateral and axial weightbearing radiographs are commonly taken by the clinician in order to properly evaluate the deformity. CT scans can also be taken which provides the clinician with a three-dimensional image that can then be used to create a three dimensional model of the foot.

Weightbearing CT images should be taken on a standard standing CT scanner or a horizontal scanner with a device that can simulate weightbearing.

2.3.1 Assessing IM and HV Angle

In the AP view of a radiograph, the IM angle and HV angle are measured to evaluate the severity of the deformity. IM angle is the angle between the long axis of the first and second metatarsal, and HV angle is the angle between the long axis of the first phalanx and first metatarsal (Figure 5). The normal IMA is <9°, and the normal HVA is <15°[17]. These radiographic angles are used to not only assess the severity of the deformity but are also important in preoperative planning.

Traditionally IMA and HVA are measured by using a pen, placing reference points, finding the axis of the targeted bone, and measuring the angle between the two axes. Having a standardized method for weightbearing radiographs and guidance when choosing reference points, is crucial in minimizing errors[18]. The AOFAS guideline for placement of reference points at the metaphyseal-diaphyseal junction of the first metatarsal, second metatarsal, and proximal phalanx is a commonly used and accurate method (Figure 5)[17].
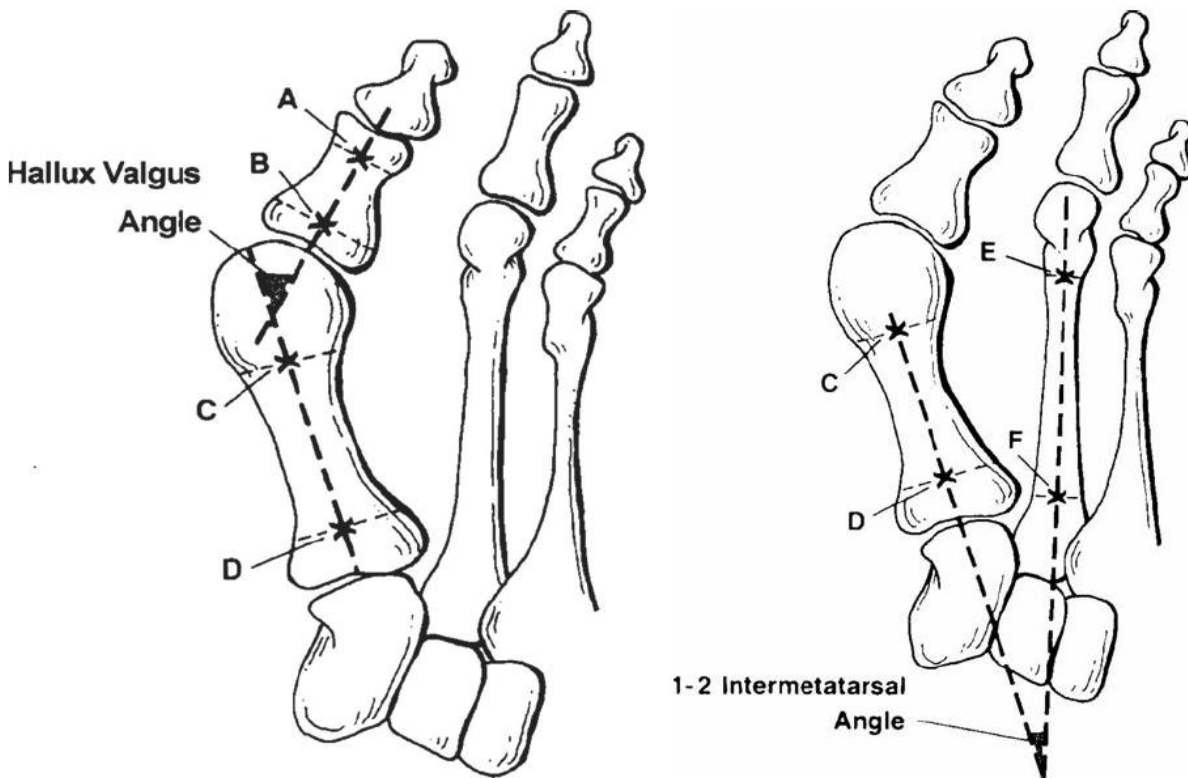
Figure 5: AOFAS guideline for placing reference points when measuring HVA and IMA

2.3.2 Assessing Sesamoid Position

Sesamoids can be assessed in the coronal view of a planar image (Figure 6), or in the tangential view of a CT scan. Normal patients have each sesamoid on a single side of the crista. Talbot and Saltzman showed that the tangential/axial sesamoid view was determined to be the most accurate view to evaluate the sesamoid position[19]. Kuwano et al. compared the sesamoid position determined from the AP view (Figure 7) to that on the tangential sesamoid view and determined that the AP view is not valid for evaluating sesamoid position[20].

Figure 6: Coronal view of the sesamoids from a planar image[19].

Figure 7: AP view of sesamoids[19].

Sesamoid grading is done according to the position of the medial sesamoid relative to the intersesamoid ridge[19]. This standardized AOFAS scale has four grades – grade 0 = sesamoid completely medial to mid-axial line, grade 1 = sesamoid less than 50% overlapping the line, grade

2 = sesamoid greater than 50% overlapping the line, and grade 3 = sesamoid completely lateral to the line (Figure 8).

Station 0   Station 1   Station 2   Station 3
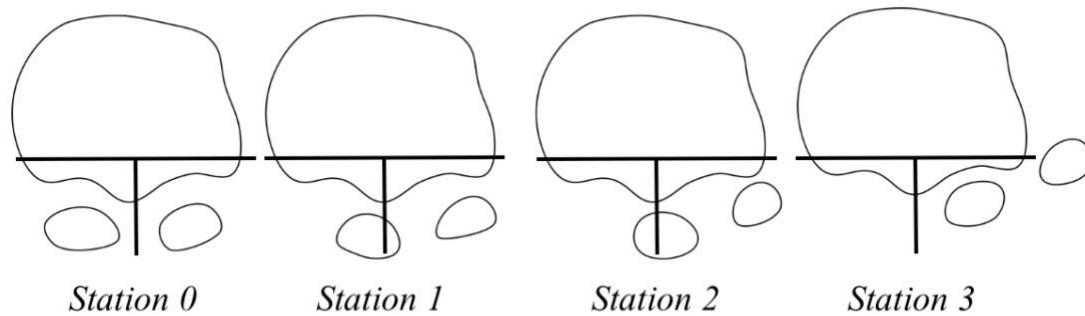
Figure 8: Sesamoid grading according to the position of the tibial sesamoid relative to the crista (intersesamoid ridge).

2.3.3 Assessing Pronation

Pronation of the first metatarsal cannot be accurately measured from a planar image. This leads to pronation not being measured clinically. An accurate way to measure pronation in CT images has not been established yet. Campbell et al. developed a point picking method that quantifies pronation of the first metatarsal relative to the second metatarsal. He created three-dimensional models of the foot from CT images and calculated the orientation of each bone by selecting landmarks on the bones. These landmarks were the (P1) most medial point of the head, (P2) most lateral point of the head, (P3) most medial point of the proximal flare, and (P4) most lateral point of the proximal flare (Figure 9). The pronation angle was calculated for the first metatarsal relative to the second metatarsal. The 3D model angles were identical to the rotations

of an aircraft: yaw (1), pitch (2), and roll (3), where yaw measured abduction/adduction, pitch measured dorsi/plantar flexion, and roll is pronation (Figure 10).

Figure 9: Landmarks selected on each 3D bone used to calculate the orientation of the bones[21].
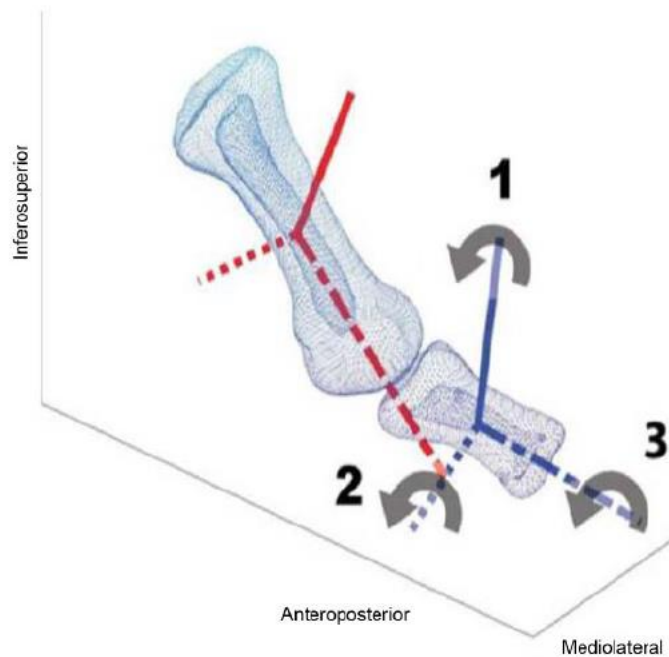
Figure 10: Calculation between the pairs of coordinate system triads were solved to calculate pronation (3)[21].

2.4 Treatment Options

Non-surgical treatments are available for hallux valgus, but the reduction of pain is temporary. One study observed bunion patients that either underwent surgical or non-surgical interventions over a span of 12 months. It was concluded that the group in which no intervention took place, experienced the same amount of pain as the non-surgical group. The surgical treatment group experienced the greatest pain reduction over the span of 12 months [22, 23]. The metatarsals, phalanx, and sesamoids are most commonly corrected to their normal alignment. The surgeries that do this are called osteotomy, arthroplasty, and arthrodesis. Part of the bone is cut and removed during an osteotomy. Inactive patients normally receive an arthroplasty, which realigns and reconstructs the joint. Severe hallux valgus can also be treated with arthrodesis, which fuses a joint with orthopaedic hardware. This hardware is normally screws and plates.

2.5 Crista and Sesamoid Literature Review

Since 1923, realignment of the sesamoids to their normal position is believed to be important for a successful bunion correction surgery. However, subluxation of the sesamoids has been found to correlate with both clinical outcomes and risk of recurrence of the HV deformity[24, 25]. Park and Lee found that immediate postoperative subluxation of the sesamoids greater than or equal to grade IV of VII following HV surgery resulted an increased likelihood of developing recurrence of their HV deformity compared to patients with less sesamoid subluxation with an

odds ratio of 9.7 [25].Therefore, understanding the relationship of sesamoid position and HV deformity may have important surgical implications.

One less studied area is the relationship of the HV deformity to degenerative changes at the sesamoid metatarsal joint. A previous study found that increasing HV deformity and sesamoid subluxation was associated with osteoarthritis of the sesamoid metatarsal joint; however, they did not objectively measure the severity of the osteoarthritic changes or investigate its association with first metatarsal pronation, which is increasingly being recognized as an important aspect of the triplanar HV deformity[26]. No studies have quantified the crista volume itself and the relationship of its volumetric change in the progression of HV.

3.0 Methods

3.1 Simulated Weightbearing Device

When evaluating a 3D deformity like HV, it is important to note that the kinematics of the foot change with loading[27]. Standard standing CT scanners are extremely expensive, therefore not every hospital has access to one. To fix this issue, we have developed a weightbearing equivalent foot pedal device that can be used in a horizontal CT scanner (Figure 11). This device allows the patient to push down on a spring loaded platform with their foot during a CT scan to simulate full weight bearing, and allows pressure distribution between the heel and forefoot. The desired load is adjusted by turning the knob on the device to half the patient's bodyweight (Figure 12). This knob adjusts two bolts that restrain the spring deflection, allowing us to choose the maximum spring deflection (half the patients body weight). The patient then pushes their foot on the plate until it compresses the springs and is stopped by two bolts. The pedal has an adjustable seat that can be moved closer or further away from the pedal, depending on the patient's height.

Figure 11: Weightbearing device used in a horizontal CT scanner.

Figure 12: Adjustable knob that is set at half the patient's body weight.

3.2 Imaging

In this research study thirty-nine HV patients and nine normal subjects underwent CT imaging with weightbearing or weightbearing equivalent (WBCT) methods after approval by the relevant Institutional Review Boards. The patients were all female, age 30-74 (HV: mean 52 SD 10 years; normal: mean 46 SD 14 years) with no pervious orthopaedic surgeries.

Working with the Hospital of Special Surgery (HSS) in New York, patients were imaged in a PedCat (CurveBeam, Inc) standing weightbearing CT scanner. Twenty-nine HV patients underwent weightbearing CT scans and X-ray imaging.

Nineteen patients, ten HV, and nine normal subjects from UPMC Passavant underwent CT imaging using a weightbearing equivalent pedal device in a LightSpeed VCT (GE, Inc.) in Pennsylvania [21, 28]. Patients were recruited from the clinics of Stephen Conti, MD, a foot and ankle surgeon at UPMC. All patients signed a consent form and were scanned in the Radiology Suite of UPMC McCandless, with the supervision of Lance Williams, MD. Along with the weightbearing CT scan, patients also underwent full weightbearing X-rays.

For the CT imaging, the patient sat in the device's chair with their knee slightly bent and pushed with their foot parallel to the pedal that was set at 75 degrees. The knob on the pedal was turned to half the patients body weight and the patient pushed on the pedal until both screws made contact with the bottom of the plate. The patient held this position until the CT scan was complete. CT scans were then examined to make sure the patient held contact with the screws throughout the entire scan (Figure 13). The patient then released pressure and sat for a non weightbearing CT scan. A set of full weightbearing X-ray images were taken in the anteroposterior direction for each patient.
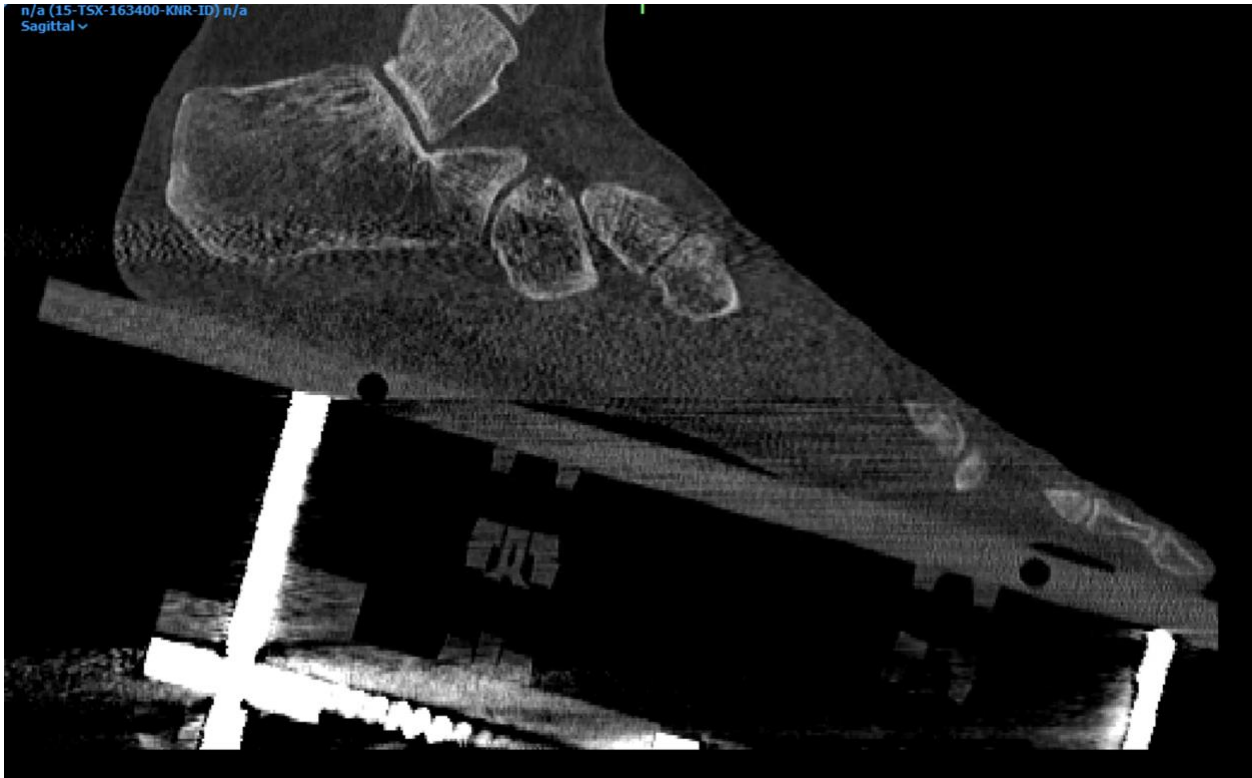
Figure 13: Sagittal view of CT scan showing that both screws are in contact with the plate.

3.3 Segmentation

Segmentation is a process of converting anatomical data from images into 3D models. Images from the CT scans were exported in a file format known as digital imaging and communications in medicine (DICOM). During a CT scan, series of X-rays are taken from different angles and then sent to a computer where they're combined to create imaged slices of the body. A DICOM data set contains identifying headers along with a series of two-dimensional images. Each two-dimensional image is a "slice" or section of the body, but when combined together can be used to construct a 3-dimensional image. These images are taken in all three planes – axial, coronal, and sagittal.

The DICOM data sequence was imported into an image processing software, Mimics (Materialise NV, Leuven, Belgium), in order to start the segmentation process. Once uploaded, Mimics calculates and creates images in the axial, coronal and sagittal direction (Figure 14).
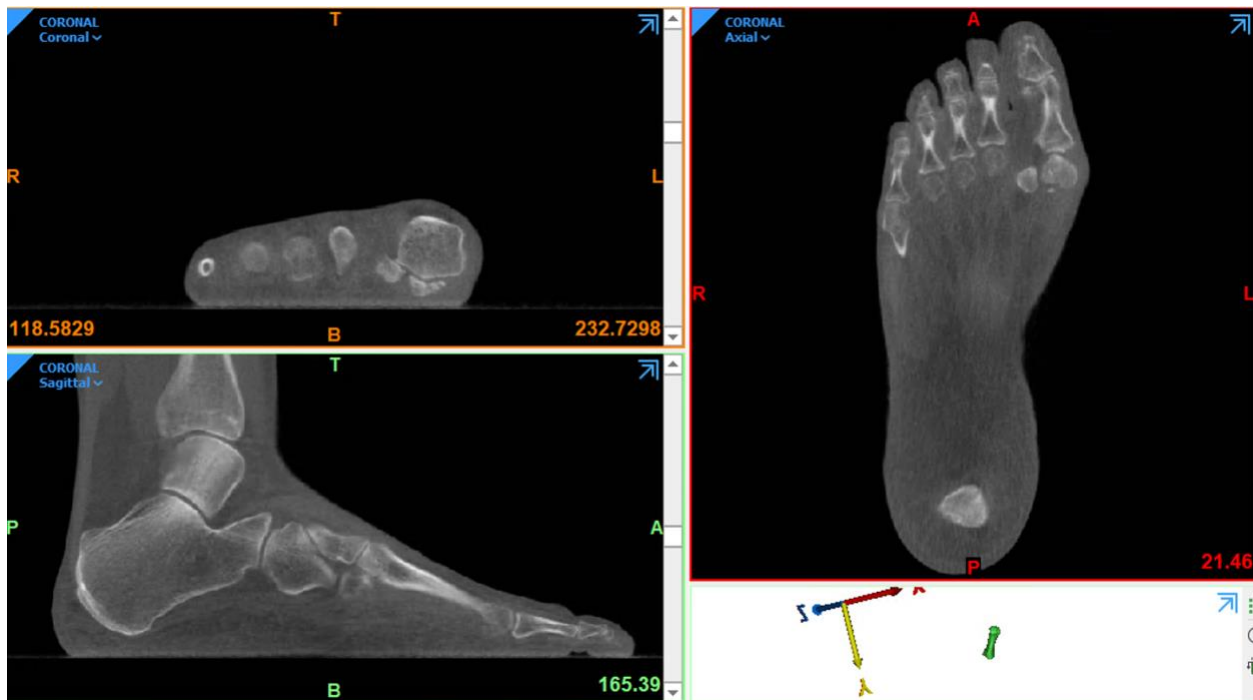
Figure 14: Axial, coronal, and sagittal views of a weightbearing CT scan in Mimics.

Manual segmentation was done by identifying the shape of a bone in a chosen slice, and outlining the group of pixels (Figure 15). Each bone is segmented slice by slice, all the way through. Using known information on the pixel size and distance between each image slice, Mimics can calculate a 3D model (Figure 16). The bone models were individually exported as .stl files to analyze later.
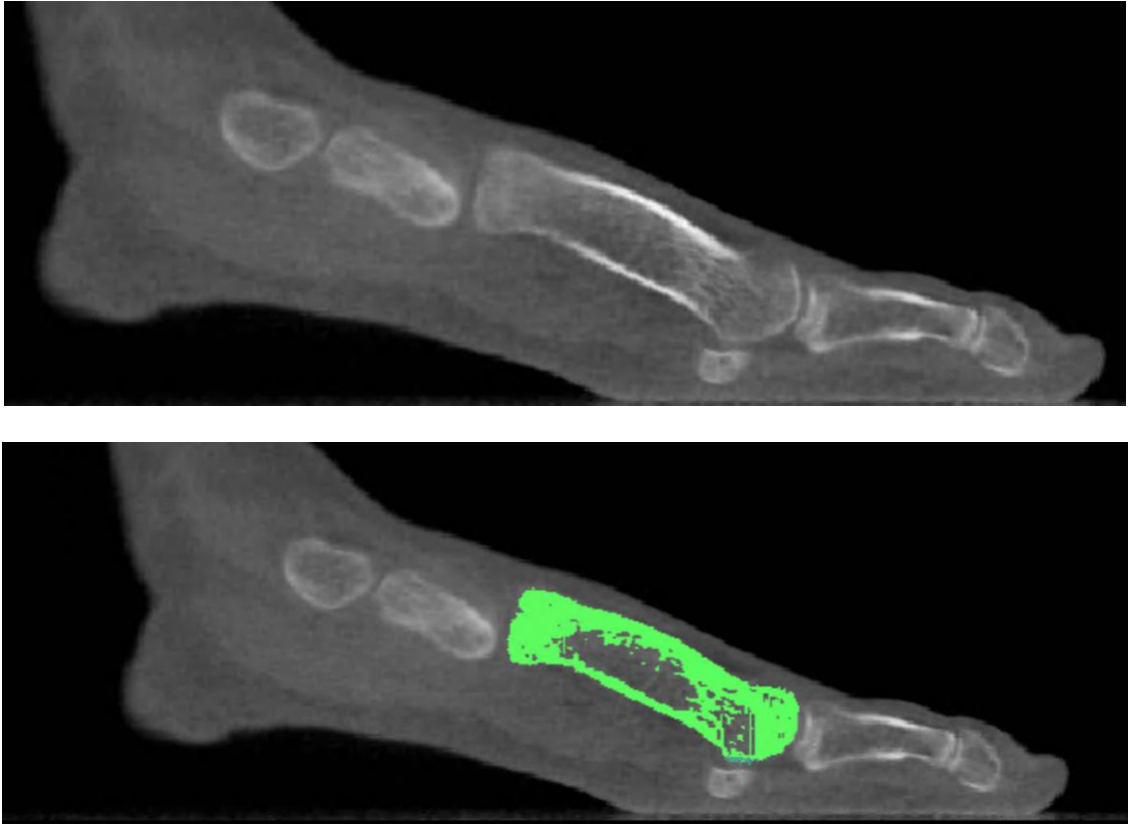
Figure 15: Manual segmentation done by outlining the 1st metatarsal.
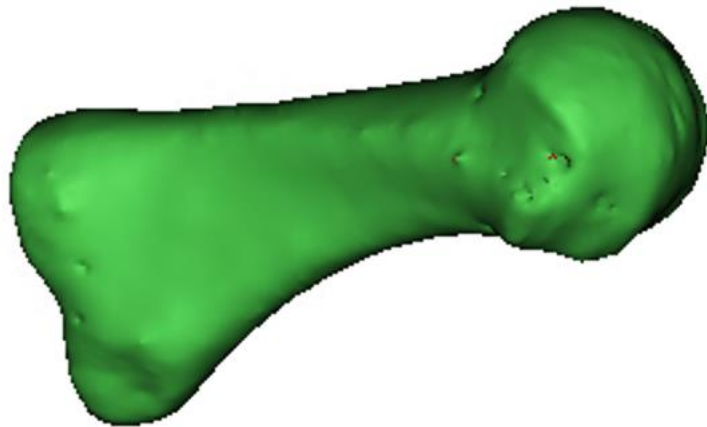
Figure 16: 3D model of the 1st metatarsal created from manual segmentation.

Although Mimics has options for auto-segmentation, they were found to be inaccurate and unreliable. Manual segmentation was accurate, but very tedious and extremely time consuming. A newer software, Disior Bonelogic (Helsinki, Findland), was used for segmentation. This software has semi-automated segmentation, which simply requires clicking on each bone once and the software does the rest (Figure 17). Using Disior, we were able to segment every bone in the foot in under an hour. After the foot was segmented, we were able to export each bone individually as an .stl file, for use in subsequent steps.
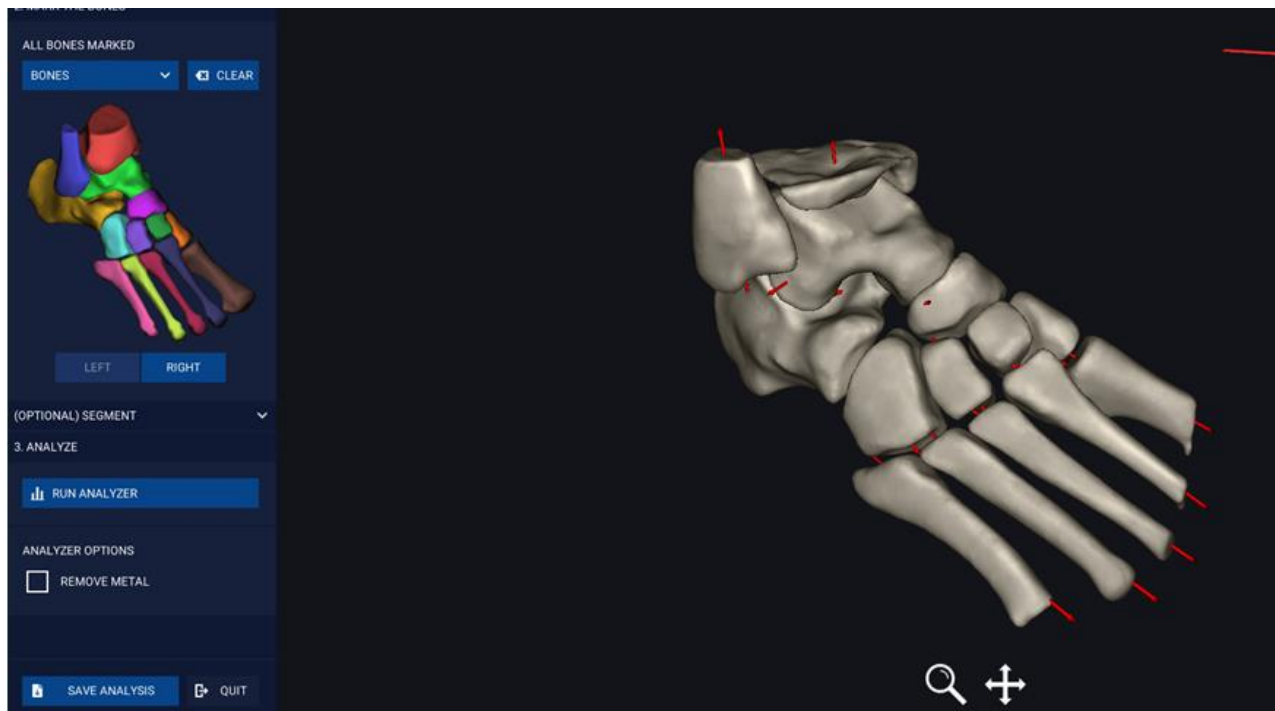
Figure 17: Semi-automated segmentation done by the program Disior Bonelogic.

Segmentation was done on five patients using the manual method and the new semi-automated method. Methods were then compared and it was determined that the semi-automated method was accurate (Figure 18).
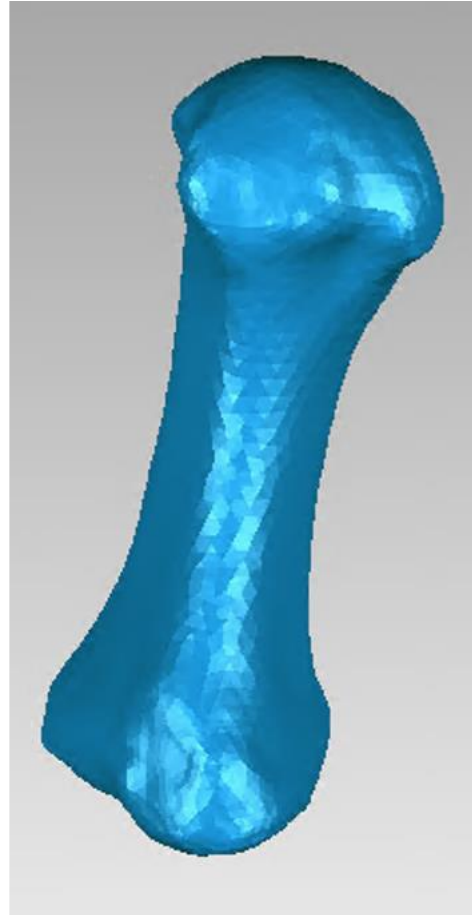
Figure 18: Segmentation of the 1ˢᵗ metatarsal done manually in Mimics (left) compared to semi-automated in Disior Bonelogic (right).

3.4 Measurements

Measurements were taken from both the weightbearing CT and X-ray. Intermetatarsal angle, hallux valgus angle, pronation angle, crista volume, and sesamoid station were recorded electronically.

3.4.1 IMA/HVA

Using the program Mimics, IMA_{1-2} and HVA were quantified from weightbearing X-rays using the standardized technique described by Coughlin[18] (Figure 19). The first metatarsal reference points are located in the metaphyeal/diaphyseal region 1-2 cm proximal to the distal articular surface and 1-2 cm distal to the proximal articular surface. The second metatarsal reference points were placed 1-2 cm proximal to the distal articular surface and 1-2 cm distal to the proximal articular surface. The proximal phalanx reference points were placed 1/2-1 cm proximal and distal to the articular surface[17]. Mimics has a built-in angle measurement that was used to connect the reference points and measure IMA_{1-2} and HVA (Figure 20).
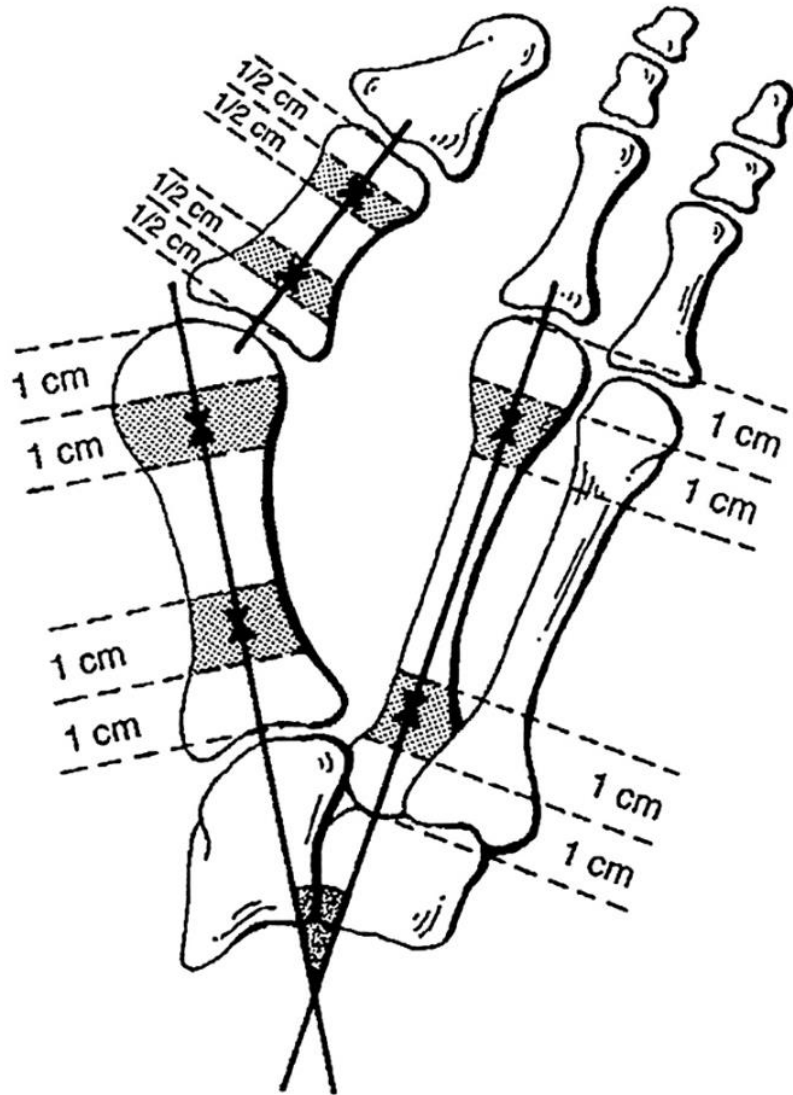
.

Figure 19: Standardized technique to measure IMA$_{1-2}$ and HVA described by Coughlin[18]
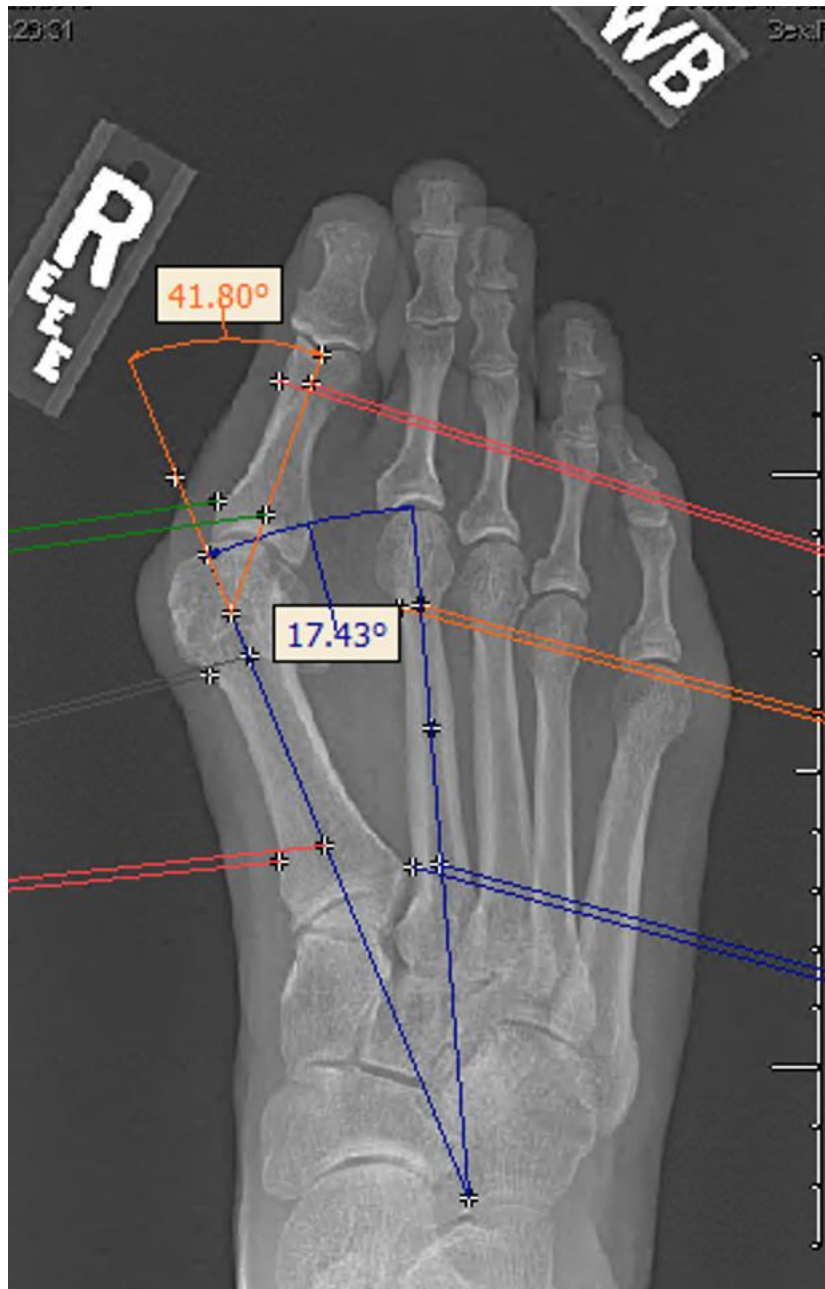
Figure 20: IMA$_{1-2}$ and HVA measured using Mimics.

3.4.2 Pronation

Using the program DISIOR, semi-automated segmentation was completed from the WBCT scans of each patient. With the 3D reconstructions from DISIOR, the pronation of the first

metatarsal was then calculated with respect to the second metatarsal. The orientations of the first and second metatarsals were determined from coordinate systems established by selecting landmarks with the program Geomagic. These landmarks (points) were exported from Geomagic and used in a calculation to geometrically determine the 3D angles using the aeronautical system of yaw-pitch-roll. The point-picking method used to calculate pronation has been previously described and validated by Campbell et al [21].

3.4.3 Crista Volume

Creation of the three-dimensional models of the CT images was performed in the coronal plane to obtain the volume of the crista. Crista cross-sections in each axial CT slice were demarcated by a line segment connecting the nadir of each sulcus on either side of the intersesamoidal crista in each slice of the WBCT image. To make this measurement consistent for every patient, the start and end point for the crista was chosen as the points at which both sulci were no longer visible. This ensured the entire structure was included. Each slice of the crista was carefully examined and highlighted from the WBCT image (Figure 21). Using the known slice thickness from the CT scan, the volume was computed.
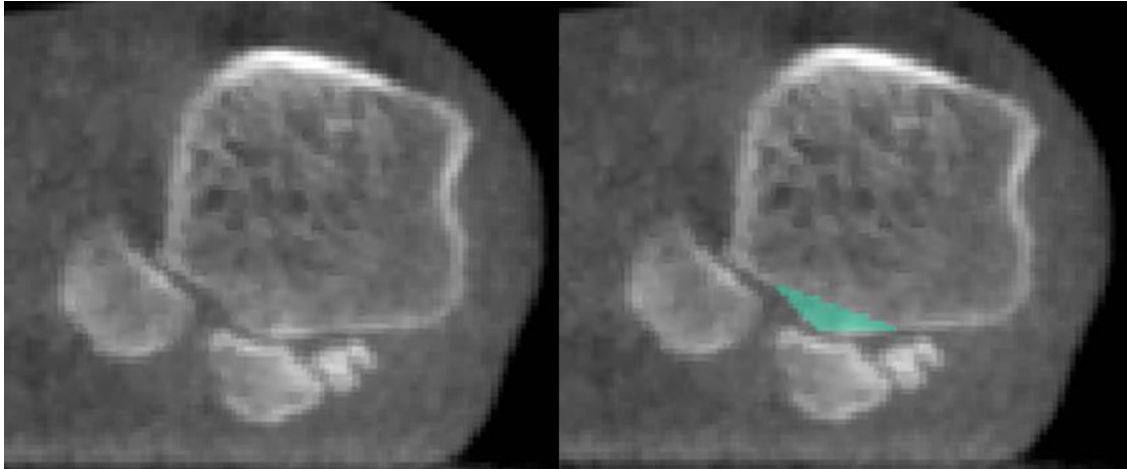
Figure 21: Calculation of the crista volume from weightbearing CT scan.

3.4.4 Sesamoid Position

Using the program Mimics, each patient's WBCT scans were uploaded and processed. Coronal, axial, and sagittal views of the WBCT scan, along with a three-dimensional reconstructive view each provided specific data about the forefoot. The coronal plane yielded a tangential sesamoid view (Figure 22), which was used to determine the sesamoid position of each patient, using the four stage AOFAS scale.
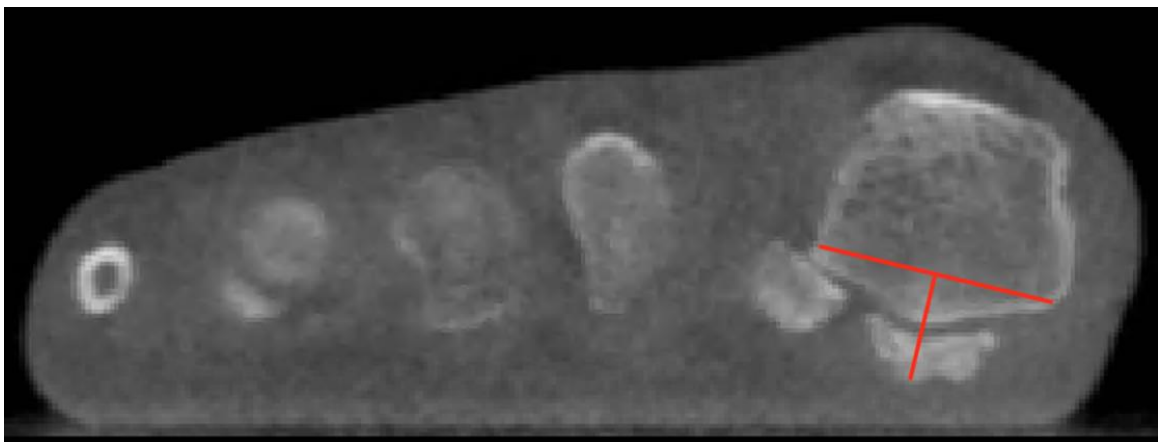
Figure 22: Tangential sesamoid view used to determine sesamoid position from weightbearing CT scan.

28

3.5 Statistical Analysis

The results from our clinical study were further analyzed using statistical analysis. The hallux valgus patient group (n = 39) was compared against the normal group (n = 9). All patients (n = 48) were grouped into four groups by their sesamoid station and compared against each other.

Parametric tests, or their non-parametric equivalent, were used to calculate the differences between groups. The mean sesamoid station was calculated and the HV and normal stations were compared using a Mann-Whitney test. T-tests were employed with a significance set at 0.05 to determine if there were differences in mean crista volume, mean IMA_{1-2}, mean HVA, and mean pronation angle between the HV and control patient groups. The sesamoid stations for all patients were grouped using the four stage AOFAS scale– and crista volume, IMA_{1-2}, HVA and pronation angle between these four groups were compared using one-way analysis of variance (ANOVA) tests. A post hoc Tukey-Kramer adjustment test was applied if significance was detected in the ANOVA tests ($p < 0.05$). Spearman's rank coefficient (Rho) was used to test the relationship of sesamoid station with the IMA_{1-2}, HVA, crista volume, and pronation angle. Linear regressions were performed to determine whether the volume of the crista was associated with the IMA_{1-2}, HVA, and the pronation angle. Statistical analysis was performed in Excel.

4.0 Results

4.1 Hallux Valgus Vs. Normal

The mean sesamoid station in HV subjects was 1.8 (range 0-3, SD 0.8) and in the non-HV group was 0.1 (range 0-1, SD 0.3). The Mann-Whitney test showed the two groups to be statistically significantly different from each other ($p < 0.001$) (Figure 23). The plots of average sesamoid station between the two groups are shown with standard deviation error bars.
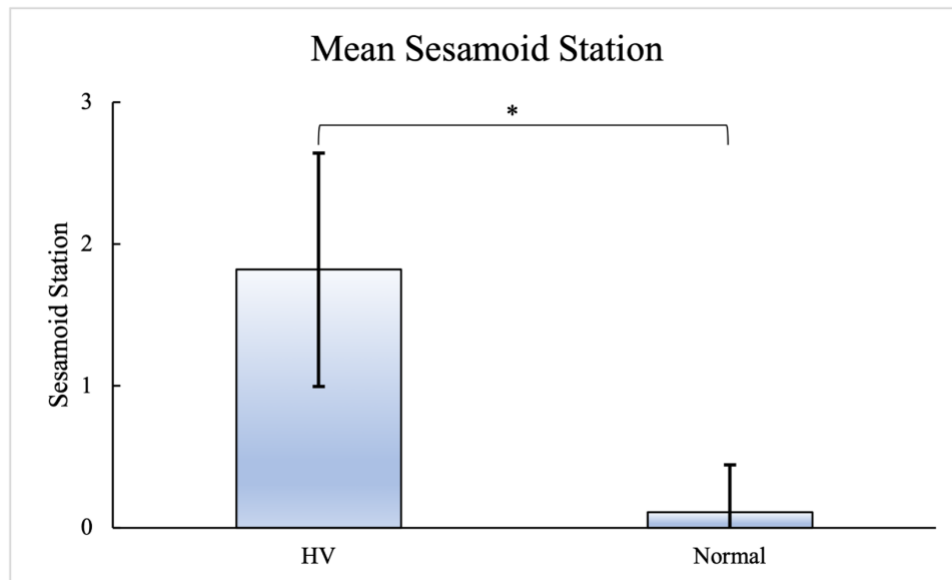
Figure 23: Mean sesamoid stations of both HV and normal

The mean crista volume in HV subjects was 80.1 mm^3 (range 18-147, SD 35 mm^3) and in normal subjects was 150.6 mm^3 (range 114-190, SD 24 mm^3), which differed significantly between the two groups ($p < 0.001$) (Figure 24). The plots of average crista volume between the two groups are shown with standard deviation error bars.
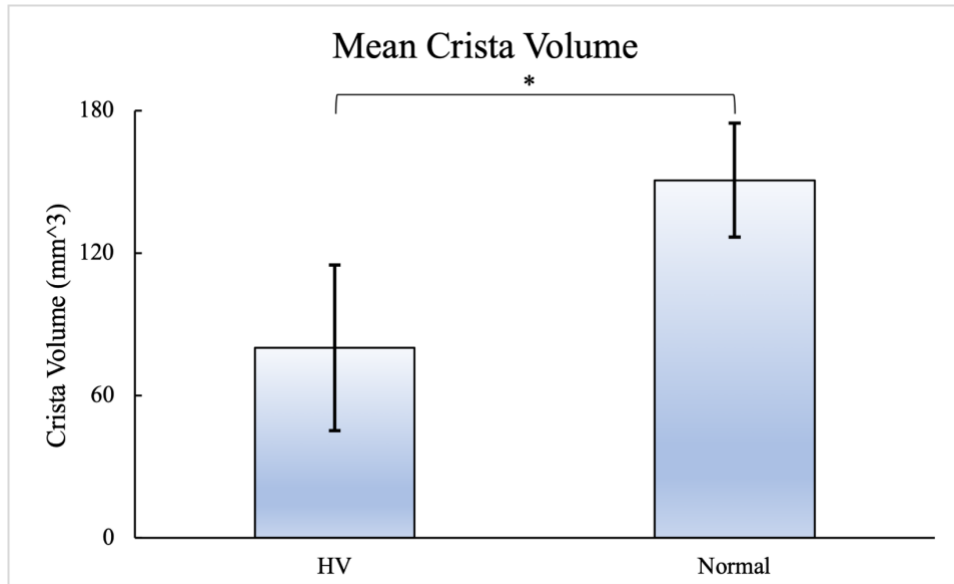
Figure 24: Mean crista volume of both HV and normal

The mean IMA in HV subjects was 15.7 degrees (range 10-22, SD 3.1 degrees) and in normal subjects was 9.4 degrees (range 7.5-11.5, SD 1.3 degrees), which differed significantly between the two groups ($p < 0.001$) (Figure 25). The plots of average IMA between the two groups are shown with standard deviation error bars.
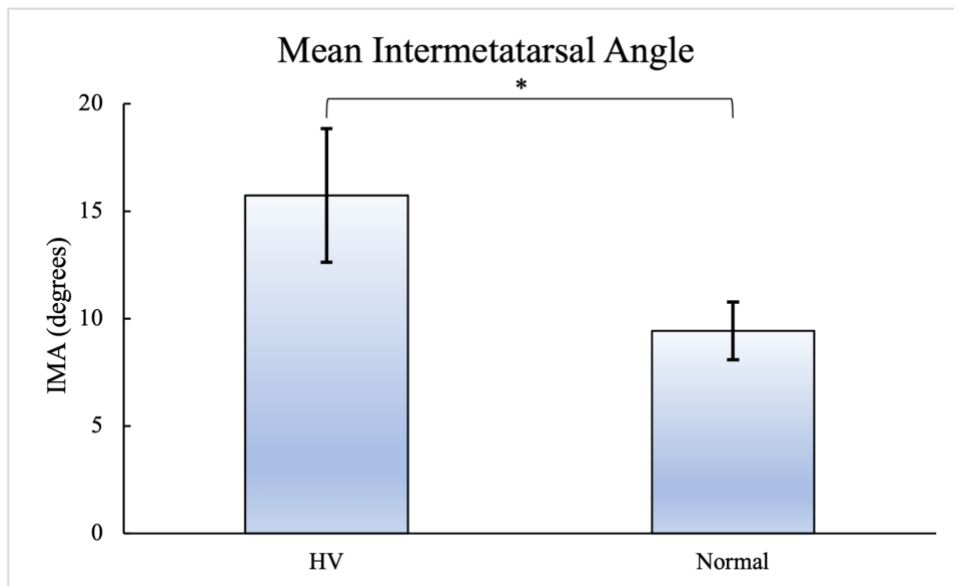
Figure 25: Mean IMA of both HV and normal

The mean HVA in HV subjects was 31.1 degrees (range 15-57, SD 9.4 degrees) and in normal subjects was 10.6 degrees (range 4.5-16, SD 3.8 degrees), which differed significantly between the two groups ($p < 0.001$) (Figure 26). The plots of average HVA between the two groups are shown with standard deviation error bars.
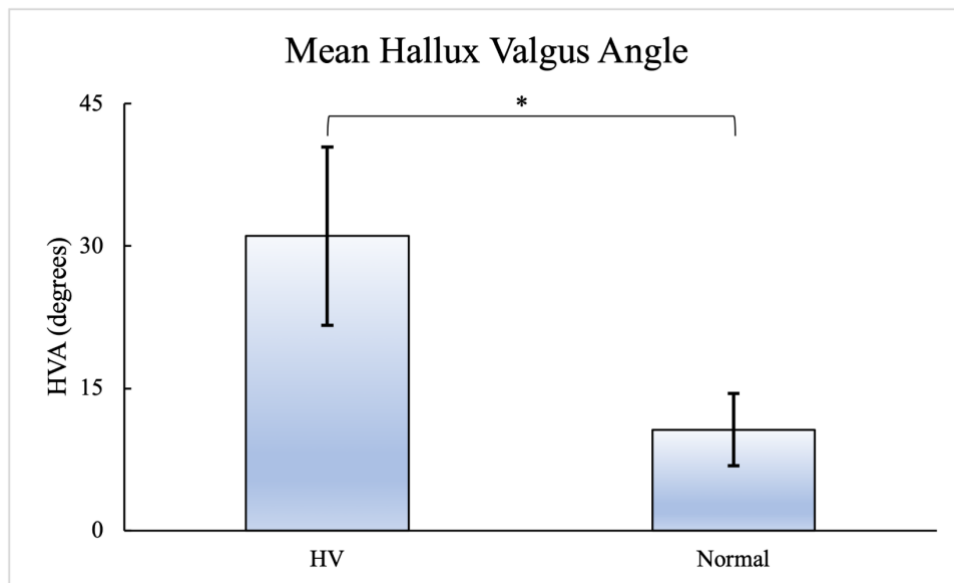
Figure 26: Mean HVA of both HV and normal

The mean pronation angle in HV subjects was 24.6 degrees (range 4-49, SD 10.2 degrees) and in normal subjects was 19.7 degrees (range 11-32, SD 6.5 degrees), which was not significantly different between the two groups ($p = 0.184$) (Figure 27). The plots of average pronation angle between the two groups are shown with standard deviation error bars.
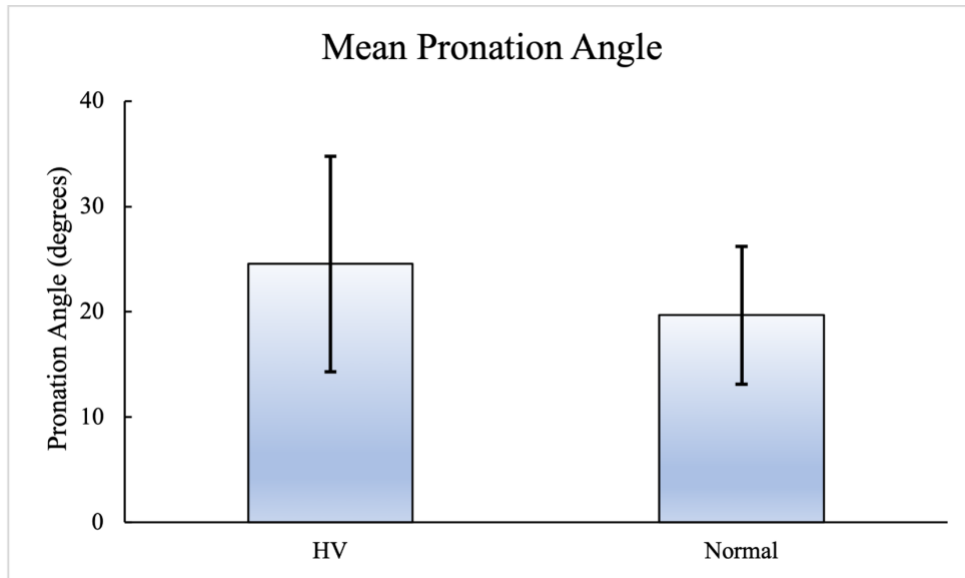
Figure 27: Mean pronation angle of both HV and normal

4.2 Grouped by Sesamoid Station

The one-way ANOVA test found the mean crista volume to be statistically different between the four sesamoid stations ($p < 0.001$). The mean values of the crista volume were 154.4 mm^3 for grade zero, 98.2 mm^3 for grade one, 78.5 mm^3 for grade two, and 44.8 mm^3 for grade three (Figure 28). The mean crista volume for each group was plotted in a bar chart with standard deviation error bars. The post hoc test showed there was significant difference in crista volume between each sesamoid grade, except for grades one and two.
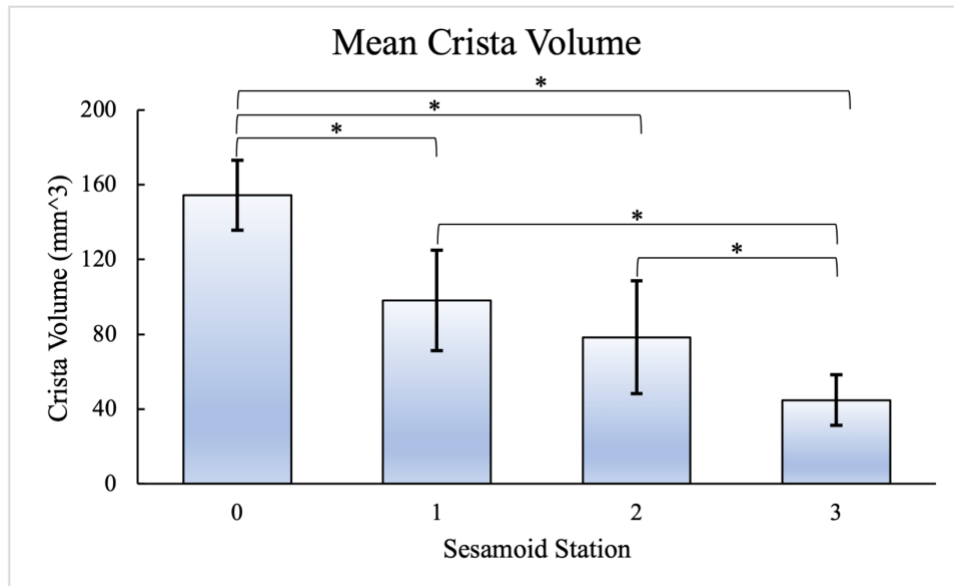
Figure 28: Crista volume averages and SD for each sesamoid station

The one-way ANOVA test found the mean IM angle to be statistically different between the four sesamoid stations ($p < 0.001$). The mean IMA values were 9.8° for grade zero, 13.4° for grade one, 16.4° for grade two, and 17.6° for grade three (Figure 29). The mean IMA for each group was plotted in a bar chart with standard deviation error bars. The post hoc test showed there was significant difference in IMA between each sesamoid grade, except for grades two and three.
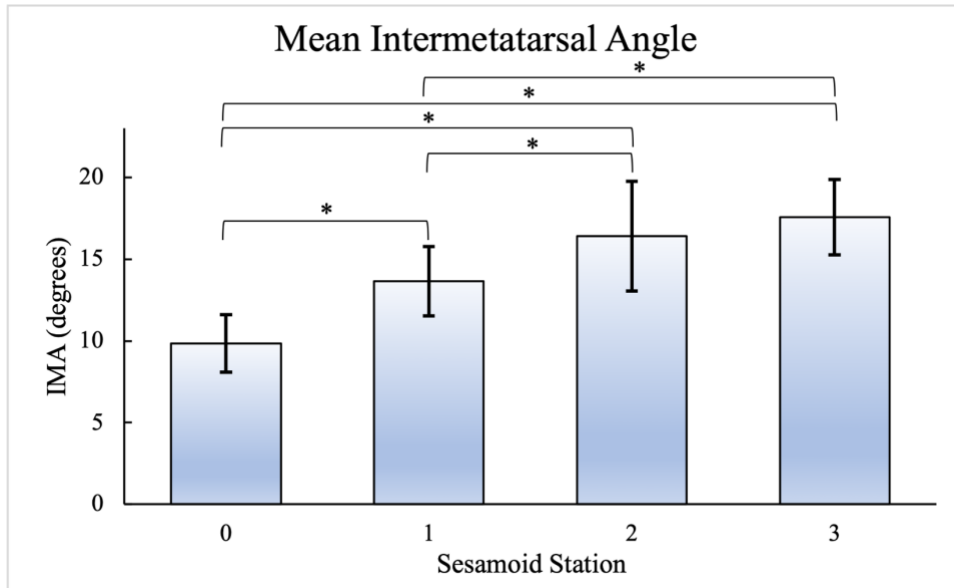
Figure 29: IMA averages and SD for each sesamoid station

The one-way ANOVA test found the mean HV angle to be statistically different between the four sesamoid stations ($p < 0.001$). The mean HVA values were 11.6° for grade zero, 24.5° for grade one, 31.3° for grade two, and 41.8° for grade three (Figure 30). The mean HVA for each group was plotted in a bar chart with standard deviation error bars. The post hoc test showed there was significant difference in HVA between each sesamoid grade.
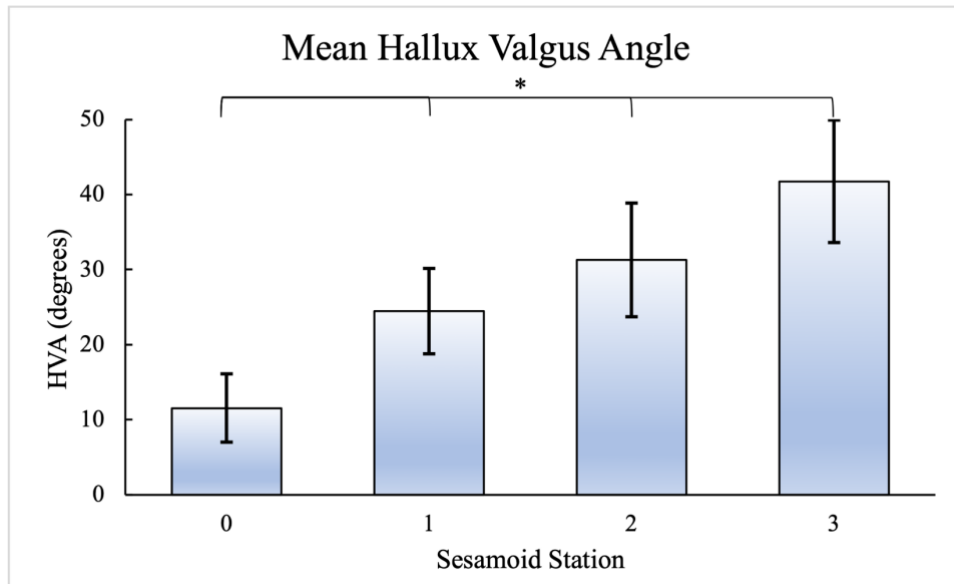
Figure 30: HVA averages and SD for each sesamoid station

The mean first metatarsal pronation angle did not differ between the four sesamoid stations ($p = 0.37$) (Figure 31). All data and tests results can be seen in Table 1.
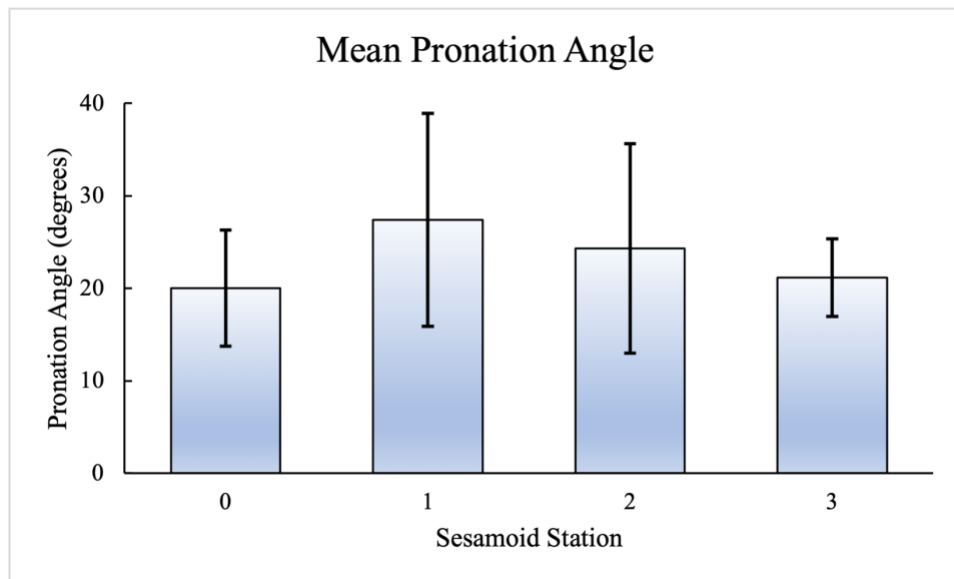
Figure 31: Pronation angle and SD for each sesamoid station.

Table 1: Average measurements by sesamoid station

Sesamoid Grade	N = 48	Crista Volume (mm³) (mean ± SD)	IMA$_{1-2}$ (degrees) (mean ± SD)	HVA (degrees) (mean ± SD)	Pronation (degrees) (mean ± SD)
Zero	10	154 ± 18.7	9.84 ± 1.8	11.6 ± 4.5	20.0 ± 6.3
One	12	98.2 ± 26.9 [A]	13.4 ± 2.1	24.5 ± 5.7	27.4 ± 11.5
Two	18	78.5 ± 30.1 [A]	16.4 ± 3.4 [B]	31.3 ± 7.6	24.3 ± 11.3
Three	8	44.8 ± 13.5	17.6 ± 2.3 [B]	41.8 ± 8.2	21.2 ± 4.2
p-value		< 0.001	< 0.001	< 0.001	0.369

Means sharing a letter are not significantly different ($\alpha = 0.05$, Tukey-Kramer adjustment on all pairwise differences).

4.3 Non-Parametric Correlations

Statistically significant correlation was noted between sesamoid station and IMA$_{1-2}$ with a Spearman's rank correlation coefficient Rho of 0.73 (*p < 0.001*). High correlation between sesamoid station and HVA was noted with Spearman's rank correlation coefficient Rho of 0.81 (*p < 0.001*). Another high correlation was noted between sesamoid station and crista volume with Spearman's rank correlation coefficient Rho of 0.80 (*p < 0.001*). No statistical significance was found between sesamoid station and pronation angle (*p* = 0.66).

4.4 Parametric Regressions

A linear regression analysis demonstrated that the crista volume was not associated with the amount of first metatarsal pronation (*p* = 0.520). However, the regression of crista volumes against the HVA demonstrated statistical significance (*p < 0.001*), with a Pearsons correlation

coefficient of 0.75. The regression of crista volumes against the IMA_{1-2} also showed statistical significance ($p < 0.001$), with a Pearsons correlation coefficient of 0.65.

5.0 Discussion

Erosion of the crista is commonly encountered in patients with HV [29]. However, no studies have sought to relate crista volume with sesamoid position and the magnitude of the HV deformity on WBCT scans. Our study found that IMA_{1-2}, HVA, and crista volume were all correlated with sesamoid position in a cohort of normal and HV patients. Increasing sesamoid station, or subluxation, was associated with greater AP radiographic deformities including IMA_{1-2} and HVA and a lower crista volume.

The sesamoid complex is connected to the second metatarsal with strong ligamentous fibers while the connection between the first and second metatarsal is weak[30]. Medial deviation of the first metatarsal over the relatively fixed sesamoids results in the sesamoid subluxation. Since the translocation of the medial sesamoid from position 0 to position 3 occurs gradually over time it is plausible that crista erosion from medial sesamoid pressure would be increased with increasing station.

Pronation of the first metatarsal, however, was not correlated with the sesamoid position. This is in keeping with studies that demonstrated poor correlation between the first and sesamoid position [31]. It also makes clear why the tangential/sesamoid view or a coronal WBCT scan view is so important in the office evaluation of HV[19]. These results are the first to demonstrate that medial sesamoid subluxation as determined by sesamoid station results in erosion of the crista. This supports the idea that sesamoid subluxation is associated with crista erosion and subsequent sesamoid metatarsal arthritis. Crista erosion may be an under-recognized component of the HV deformity.

Katusi et al. looked at the relationship between degenerative changes of the sesamoid metatarsal joint and lateral shift of the sesamoids in 269 feet with hallux valgus using simulated WBCT scans [26]. Degenerative changes of the sesamoid metatarsal joint were categorized into osteoarthritis negative and osteoarthritis positive groups. Patients in the osteoarthritis negative group had an intact crista without bony erosion or cystic lesions; whereas, patients in the osteoarthritis positive group had erosive or cystic changes of the sesamoid metatarsal joint or erosion of the crista on simulated WBCT scans. As the sesamoids became more subluxated, the percentage of patients with osteoarthritic changes of the sesamoid metatarsal joint increased. Additionally, the mean HVA and IMA increased with increasing grades of sesamoid subluxation. This study was limited by the binary classification of osteoarthritis changes of the sesamoid metatarsal joint. However, these findings are consistent with the findings of our study. Degenerative changes of the sesamoid metatarsal joint as determined from decreasing crista volumes in our study were correlated with increased sesamoid subluxation. Additionally, increasing sesamoid subluxation was also associated with increased HVA and IMA deformities.

Chen et al. investigated the role of postoperative tibial sesamoid position on patient-reported outcomes using the visual analog scale, the American Orthopaedic Foot & Ankle Society Hallux Metatarsophalangeal-Interphalangeal Scale, and patient satisfaction following surgery for hallux valgus deformity in 250 feet[24]. They used the Hardy and Clapham tibial sesamoid position classification system to grade sesamoid position (grades I - VII) based on the longitudinal axis of the first metatarsal. Patients with higher postoperative sesamoid position grades (grades V – VII) who had more subluxation of the sesamoid were considered "outliers." They found that the VAS score was one point better and the AOFAS Hallux score was 6 points better in the normal group compared to the outliers group. Additionally, patients in the outliers group were more likely

to be dissatisfied with their surgery than patients in the normal group. The authors concluded that postoperative sesamoid position influenced two-year postoperative patient-reported outcomes and that patients with more severely subluxated sesamoids had worse clinical outcomes.

However, another study found that AP radiographs were not adequate to assess sesamoid subluxation [32]. Kim et al. compared sesamoid position on weightbearing AP radiographs using the Hardy and Clapham tibial sesamoid position classification to the position of the sesamoids on simulated WBCT scan coronal views in 166 feet with hallux valgus. They described a group of patients who had "pseudo-sesamoid subluxation," which was defined as a high-grade sesamoid position (grades V – VII) on the AP radiograph but a grade 0 (reduced) sesamoid subluxation on the axial WBCT view. The authors reported that "pseudo-subluxation" of the sesamoids occurred in 25.9% of patients and may be due to increased first metatarsal pronation. Consequently, weightbearing AP radiographs may not be a reliable tool to assess postoperative sesamoid position.

Patient discomfort from HV has been attributed to shoe fit, the medial eminence prominence, capsuloligamentous stretch around the first metatarsophalangeal joint, and incongruency of the first MTPJ [14, 33]. Few authors have discussed metatarsosesamoid changes as the primary source of discomfort. While the former theories have been promoted by surgeons to their patients, there have been no demonstrated anatomic descriptions of disease in the tissues thought to cause pain. Treatments have been based on a surgeon's concept of the disease; for example, if ill-fitting footwear was thought to cause pain then the logical treatment would be for the patient to obtain a larger shoe. The senior author's opinion is that patients see their enlarged medial eminence and associate the metatarsosesamoid pain with it. In almost all instances, palpation of the medial eminence reveals no tenderness however palpating the medial sesamoid while dorsiflexing and plantarflexing the great toe elicits significant discomfort.

There are a few limitations to this study. First, our study is limited by the small sample size of the HV patients (n=39) and normal control patients (n=10). It may be that a greater number of patients would reveal a relationship between first metatarsal pronation and crista volume or sesamoid station; however, our work is in line with previous work demonstrating no relationship between sesamoid position and pronation. Additionally, we used two different types of WBCT scan devices including performing simulated WBCT scans in a device that has been previously used [21] and using a standing WBCT scan device. This may result in differences between sesamoid subluxation between the two groups. Finally, the clinical implications of decreased crista volume are unclear at this time. While we believe that decreased crista volume and degenerative changes of the sesamoid metatarsal joint is associated with increased pain and more debilitating symptoms, we were not able to correlate these findings with clinical outcome scores.

In this paper we have shown that as the IMA_{1-2} and HVA increase, the sesamoid station increases with a corresponding decrease in crista volume. Crista volume reduction is a proxy for a measure of crista erosion. The relationship with the IMA_{1-2}, HVA, and crista volume is expected because a large HVA and IMA_{1-2} would translocate the sesamoids causing crista erosion. This would suggest that general principles of orthopaedics should apply to HV care, and surgeons should consider realigning the sesamoids to prevent further crista erosion and degenerative changes of the sesamoid metatarsal joint.

Bibliography

1. Nix, S., M. Smith, and B. Vicenzino, *Prevalence of hallux valgus in the general population: a systematic review and meta-analysis.* J Foot Ankle Res, 2010. **3**: p. 21.

2. Menz, H.B. and S.R. Lord, *Gait instability in older people with hallux valgus.* Foot Ankle Int, 2005. **26**(6): p. 483-9.

3. Menz, H.B. and S.R. Lord, *The contribution of foot problems to mobility impairment and falls in community-dwelling older people.* J Am Geriatr Soc, 2001. **49**(12): p. 1651-6.

4. Fraissler, L., et al., *Treatment of hallux valgus deformity.* EFORT Open Rev, 2016. **1**(8): p. 295-302.

5. Kilmartin, T.E., *Revision of failed foot surgery: a critical analysis.* J Foot Ankle Surg, 2002. **41**(5): p. 309-15.

6. COUGHLIN, M.J., *Instructional Course Lectures, The American Academy of Orthopaedic Surgeons - Hallux Valgus*†.* JBJS, 1996. **78**(6): p. 932-66.

7. ; Available from: https://athletics.fandom.com/wiki/Planes_of_Motion#cite_ref-gov_1-0.

8. Osteomyoamare. Available from: https://commons.wikimedia.org/wiki/File:Anatomical_Directions.png.

9. Bonney, G. and I. Macnab, *Hallux valgus and hallux rigidus; a critical survey of operative results.* J Bone Joint Surg Br, 1952. **34-b**(3): p. 366-85.

10. Sim-Fook, L. and A.R. Hodgson, *A comparison of foot forms among the non-shoe and shoe-wearing Chinese population.* J Bone Joint Surg Am, 1958. **40-a**(5): p. 1058-62.

11. Nix, S.E., et al., *Gait parameters associated with hallux valgus: a systematic review.* J Foot Ankle Res, 2013. **6**(1): p. 9.

12. Menz, H.B., et al., *Epidemiology of Shoe Wearing Patterns Over Time in Older Women: Associations With Foot Pain and Hallux Valgus.* J Gerontol A Biol Sci Med Sci, 2016. **71**(12): p. 1682-1687.

13. Aseyo, D. and H. Nathan, *Hallux sesamoid bones. Anatomical observations with special reference to osteoarthritis and hallux valgus.* Int Orthop, 1984. **8**(1): p. 67-73.

14. Mann, R.A. and M.J. Coughlin, *Hallux valgus--etiology, anatomy, treatment and surgical considerations.* Clin Orthop Relat Res, 1981(157): p. 31-41.

15.   Shamus, J., et al., *The effect of sesamoid mobilization, flexor hallucis strengthening, and gait training on reducing pain and restoring function in individuals with hallux limitus: a clinical trial.* J Orthop Sports Phys Ther, 2004. **34**(7): p. 368-76.

16.   Robinson, A.H. and J.P. Limbers, *Modern concepts in the treatment of hallux valgus.* J Bone Joint Surg Br, 2005. **87**(8): p. 1038-45.

17.   Coughlin, M.J., C.L. Saltzman, and J.A. Nunley, 2nd, *Angular measurements in the evaluation of hallux valgus deformities: a report of the ad hoc committee of the American Orthopaedic Foot & Ankle Society on angular measurements.* Foot Ankle Int, 2002. **23**(1): p. 68-74.

18.   Srivastava, S., N. Chockalingam, and T. El Fakhri, *Radiographic angles in hallux valgus: comparison between manual and computer-assisted measurements.* J Foot Ankle Surg, 2010. **49**(6): p. 523-8.

19.   Talbot, K.D. and C.L. Saltzman, *Assessing sesamoid subluxation: how good is the AP radiograph?* Foot Ankle Int, 1998. **19**(8): p. 547-54.

20.   Kuwano, T., et al., *New radiographic analysis of sesamoid rotation in hallux valgus: comparison with conventional evaluation methods.* Foot Ankle Int, 2002. **23**(9): p. 811-7.

21.   Campbell, B., et al., *Pilot Study of a 3-Dimensional Method for Analysis of Pronation of the First Metatarsal of Hallux Valgus Patients.* Foot Ankle Int, 2018. **39**(12): p. 1449-1456.

22.   Torkki, M., et al., *Surgery vs orthosis vs watchful waiting for hallux valgus: a randomized controlled trial.* Jama, 2001. **285**(19): p. 2474-80.

23.   Torkki, M., et al., *Hallux valgus: immediate operation versus 1 year of waiting with or without orthoses: a randomized controlled trial of 209 patients.* Acta Orthop Scand, 2003. **74**(2): p. 209-15.

24.   Chen, J.Y., et al., *Tibial Sesamoid Position Influence on Functional Outcome and Satisfaction After Hallux Valgus Surgery.* Foot Ankle Int, 2016. **37**(11): p. 1178-1182.

25.   Park, C.H. and W.C. Lee, *Recurrence of Hallux Valgus Can Be Predicted from Immediate Postoperative Non-Weight-Bearing Radiographs.* J Bone Joint Surg Am, 2017. **99**(14): p. 1190-1197.

26.   Katsui, R., et al., *Relationship Between Displacement and Degenerative Changes of the Sesamoids in Hallux Valgus.* Foot Ankle Int, 2016. **37**(12): p. 1303-1309.

27.   Fuhrmann, R.A., F. Layher, and W.D. Wetzel, *Radiographic changes in forefoot geometry with weightbearing.* Foot Ankle Int, 2003. **24**(4): p. 326-31.

28.   Fadle, A.A., et al., *A simple foot pedal device in a horizontal bore imaging facility replicates weightbearing outcomes for Hallux Valgus patients.* Foot Ankle Surg, 2020. **26**(3): p. 320-324.

29.   Dedmond, B.T., J.W. Cory, and A. McBryde, Jr., *The hallucal sesamoid complex.* J Am Acad Orthop Surg, 2006. **14**(13): p. 745-53.

30.   Sarrafian, S.K., *Anatomy of the foot and ankle: descriptive, topographic, functional.* 1993: Lippincott Williams & Wilkins.

31.   Conti, M.S., et al., *Effect of the Modified Lapidus Procedure on Pronation of the First Ray in Hallux Valgus.* Foot Ankle Int, 2020. **41**(2): p. 125-132.

32.   Kim, Y., et al., *A New Measure of Tibial Sesamoid Position in Hallux Valgus in Relation to the Coronal Rotation of the First Metatarsal in CT Scans.* Foot Ankle Int, 2015. **36**(8): p. 944-52.

33.   Piggott, H., *The natural history of hallux valgus in adolescence and early adult life.* The Journal of Bone and Joint Surgery. British volume, 1960. **42**(4): p. 749-760.